MEASUREMENTS OF THE 1MM RECEIVER OPTICS

Dick Plambeck
Radio Astronomy laboratory, University of California, Berkeley, CA, 94720
March 2000

ABSTRACT

When 1mm receivers were first installed on the BIMA antennas in October 1997, the aperture efficiencies were found to be unexpectedly poor. Lab measurements of the 1mm receiver optics finally identified the problem – two of the optical components in each dewar, a lens at the feedhorn aperture and a flat 50 K window used as an infrared filter, had been machined from defective rods of extruded Teflon (PTFE). These rods were slightly porous along their central axes, leading to a radial gradient in refractive index which corrupted the receiver beam pattern.

When the defective components were replaced with lenses and windows fabricated from Teflon plate, the measured beam patterns closely matched those predicted by Gaussian beam analysis, and the aperture efficiencies improved dramatically. The new lenses were antireflection-coated by drilling a grid of holes into each surface, rather than by cutting circular grooves into the surface. In this way the refractive index of the antireflection layer is insensitive to polarization.

This memo summarizes the optical layout of the BIMA antennas and receivers, gives a brief history of the 1mm aperture efficiency problem, and describes lab tests and theoretical modelling of the 1mm optical components. Section 7 discusses the antireflection coating on the new lenses.

1. Background: BIMA telescope and receiver optics

Figure 1 shows the optical layout of the BIMA antennas. The receivers are mounted at the f/4.94 Cassegrain focus. The receiver optics (Figures 2,3) were designed by John Lugten, following the precepts outlined by Padman, Murphy, & Hills (1987). For each frequency band, two lenses are used to couple radiation from the Cassegrain focus to the receiver feed horn. The first lens, which doubles as the dewar vacuum window, refocusses the incoming beam to form an image of the telescope primary mirror at the feed horn aperture. The second lens, mounted on the 15 K radiation shield just in front of the feed horn, matches this flat image to the curved wavefront of the feed horn. The incoming beam also passes through a flat Teflon window, mounted on the 50 K radiation shield, which serves as an infrared filter. Lens dimensions are given in Figure 4.

Careful calculations of the expected telescope aperture efficiencies (including the effects of spillover, central blockage, feedleg blockage, surface roughness, gaps between panels, and scattering by panel adjusting screws) are summarized in Table 1 of Lugten (1995) – the expected values are 0.77 at 100 GHz and 0.73 at 230 GHz.

2. The 1mm aperture efficiency problem

When 1mm receivers were first installed on the telescopes in 1997 Oct, we were surprised to find that at 1mm the optimum subreflector focus positions were offset by -1.0 mm (subreflector moved away from the primary mirror) from the corresponding 3mm settings. Although this seems like a small shift, it moves the Cassegrain focus forward (toward the subreflector) by $(m^2+1)\times$1mm $\sim$ 5.5 inches, where $m = 11.76$ is the magnification ratio of the secondary (Schroeder 1987, pp. 16-20). Worse, the measured 1mm aperture efficiencies were only 0.3 to 0.35, less than half the expected value, even with the subreflectors refocussed for optimum gain.

Tests over the next few months found no obvious cause for the low efficiencies. The 1mm lenses appeared to be machined to the correct figure, and a ray tracing study (Hudson 1998) indicated that subreflector misaligment was unlikely to be a problem. Thus, in May 1998 we installed a 230 GHz transmitter at the Hat Creek Rim lookout tower and made holographic measurements of several antennas. These indicated that the antenna illumination pattern was much narrower than expected (Figure 5), and had a mysterious $\sim$ 2 radian phase jump at about half the radius of the antenna.

3. Lab test setup

Because the holography data pointed to a flaw in the feed horn or receiver optics, I set up a transmitter and receiver in the lab in July 1998 to measure the beam pattern of a 1mm receiver. Figure 6 shows a block diagram of this setup. The transmitter frequency was 225.02 GHz. This was downconverted to 150 MHz in the receiver, then mixed with 150.000400 MHz to obtain a 400 Hz fringe which could be synchronously detected. By stepping the phase of the receiver's first local oscillator in 90 degree increments, I measured the cos, sin, $-cos$, and $-sin$ components of the fringe, hence its amplitude and phase. The dynamic range was approximately 100:1 in voltage, thus 40 dB in power. All measurements were made with the receiver optics at room temperature.

The transmitter was mounted on a (makeshift) computer-controlled translation stage positioned 40 to 60 inches away from the receiver. It was stepped through the receiver beam in 0.1 inch increments over a 25 inch range. Scans were made only through the midplane of the beam pattern in the azimuthal direction, perpendicular to the E-field polarization. No attempt was made to measure the cross polarized power. Each scan required 15 to 20 minutes.

Data were taken with program */prog/test/beampat2.c*, which produced a file containing the translation stage position, cosine and sine amplitudes, and fringe amplitude and phase. This file was passed to program */prog/test/beampat3.c*, which normalized the peak amplitude to 1.0, offset the x-coordinate to center the peak at 0.0, unwrapped the fringe phase, and computed the phase residual after removing a spherical cap of specified radius. A data analysis example is shown in Figure 7.

4. Theoretical modelling

The measured beam patterns were compared with theoretical patterns predicted on the basis of Gaussian beam analysis, generated with Jerry Hudson's *Geebeams* software package. Appendix A lists the script used to generate the theoretical patterns shown in this memo.

The models start with the E-field across the feed horn aperture (Wylde 1984),

$$E_y(r) = AJ_0\left(2.405\frac{r}{a}\right) exp\left(\frac{-ik_0 r^2}{2R_{cap}}\right), \qquad r < a,$$

where $a = 0.345''$ is the radius of the aperture of our 1mm horn and $R_{cap} = 1.65''$ is the radius of curvature of a spherical cap centered at the apex of the horn. We expand this function in a set of Gaussian modes, arbitrarily choosing beamwaist $w = 0.6437a$ in order to maximize the power in the fundamental Gaussian mode. From the feed horn, the beam passes through the (plano-convex) horn lens and the (convex) dewar lens. For the *Geebeams* analysis, each curved lens surface was treated as a thin lens of focal length $R/(n-1)$, where R is the radius of curvature of the surface (fit by eye to a plot of the surface) and $n = 1.442$ is the assumed room temperature refractive index of Teflon. These focal lengths are listed in the caption of Figure 4.

5. Problem #1: defective 50 K windows

Measurements of the 1mm feed horn by itself, with no lenses installed, quickly ruled it out as the cause of the problem. As shown in Figure 8, its beam pattern closely matches theory. On the other hand, the pattern of the full 1mm optics package (Figure 9) was much narrower than expected, with the same mysterious phase jump measured holographically on the antennas.

The receiver beam pattern improved dramatically when the flat 50 K window was removed. Figure 10 shows why: the phase delay through this flat slab of Teflon is 20% smaller at its center, presumably because it was cut from an extruded rod of Teflon which was slightly porous along the central axis. When held in front of a bright light, a dark area was evident at the center of the defective windows.

New 50 K windows were machined from a flat plate of Teflon. Scans similar to the one in Figure 10 showed that the refractive index of the new windows was constant within the measurement accuracy, $\sim 5\%$. The beam pattern of the complete system with one of the new windows installed is shown in Figure 11. Although improved, the beam pattern is narrower than expected, and its center of curvature is not at the predicted position. Since there was little time to investigate these discrepancies before the mm receivers were reinstalled on the telescopes in Sep 98, we went ahead and replaced all the 1mm 50 K windows. All but one of these windows were found to be bad, as evidenced by the dark area at the center; only the window on antenna 6 was OK. With the dewars open we also checked the 50 K windows in the 3mm band – two of these also were found to be defective and were replaced. Presumably these had caused no obvious problems because of the longer wavelength.

With the new windows in place, a limited set of observations were done to find the best focus position; it seemed to be unchanged, at -1.0 mm from the optimum 3 mm focus. (The calculations described in Section 8 show that the optimum focus should have shifted closer to the 3mm focus). The aperture efficiencies improved somewhat, to 0.4 to 0.45.

6. Problem #2: defective horn lenses

In Dec 98 I did further modelling to try to understand the discrepancies between the measured and expected beam patterns. Remarkably, the models reproduced almost every feature of the measured beam patterns when I added a "cusp" to the refractive index of the horn lenses, similar to that measured for the 50 K windows. As indicated in Appendix A, the "cusp" was included by computing the complex E-field at the lens, multiplying by the cusp phase term, then recomputing the Gaussian mode coefficients. Dashed curves in Figures 9, 11, and 12 show the beam patterns predicted by these models.

We then machined a new horn lens from Teflon sheet, exactly to the dimensions of the old lens. With the new lens in place, the measured beam patterns – of the horn + horn lens, and of the entire optical system – closely matched the desired patterns (Figures 12 and 13). Accordingly, we machined a new set of horn lenses for the 1mm band. Although beam pattern measurements at 3mm showed no significant problems with the old 3mm lenses, we decided to make a new set of 3mm horn lenses as well, since this allowed us to correct a known flaw in antireflection coatings on the lenses, discussed in section 7 below.

The new lenses were machined on our Tree milling machine using Dynapath scripts generated by program *plambeck/optics/hornlens.c*. All the 1mm and 3mm lenses on the telescopes were replaced by 1 March 1999. With new new lenses in place, there is no longer a focus offset between the 1mm and 3mm bands, and the aperture efficiencies are much closer to their nominal values (Figure 16).

7. Antireflection coating with a grid of holes

The old lenses were antireflection coated by cutting a series of concentric grooves into their surfaces; for the 1mm lenses the grooves were $0.010''$ wide, $0.0102''$ deep, with pitch $0.020''$. Although this is the conventional method of antireflection coating plastic lenses at microwave frequencies, it has the disadvantage that the refractive index of the matching layer differs depending on whether the E-field is parallel or perpendicular to the grooves (this is, after all, how one makes polarization plates):

$$n_{\|} = \sqrt{\frac{\epsilon+1}{2}}, \qquad n_{\perp} = \sqrt{\frac{2\epsilon}{\epsilon+1}}$$

Thus, for Teflon ($\epsilon = 2.08$) the matching layer has refractive index 1.24 where the grooves are parallel to the E-field, 1.16 where they are perpendicular. Ideally, the matching layer is $\lambda/4$ thick, with dielectric constant $\sqrt{2.08}$, and hence refractive index 1.20.

Although the grooved surfaces do an adequate job of antireflection coating the lens, John Lugten has pointed out that they cause an undesirable systematic variation in delay through the lens. For vertically polarized signals, the delay through the top and bottom of the lens is smaller than through the sides (Figure 14). Since the horn lens lies close to an image of the telescope primary mirror, there is a one-to-one correspondence between points on the lens and points on the primary mirror. Thus, if one makes a holographic measurement of the antenna surface through the grooved lens, the top and bottom edges of the antenna will appear – incorrectly – to be folded inward. Since we adjusted the panels on each antenna on the basis of such holographic measurements, we would have inadvertently distorted the dish surface to remove this pattern. This distortion correctly compensates the delay in the matching grooves only at the frequency for which the holography was done.

In our case, the panels were set using holography at 90 GHz. The $d = 0.024''$ deep grooves on each side of the 3mm horn lens produce a peak-to-peak path difference $(n_{\|} - n_{\perp})(2d) = 97$ micron across the telescope aperture, whereas the corresponding path difference for the 1mm lenses is only 41 microns. Thus, setting the panels perfectly at 3mm produces a 56 micron peak-to-peak (28 micron rms) surface error) at 1mm.

Since we used a milling machine to manufacture the lenses, it was practical to antireflection coat them by drilling a regular array of holes into the surface. The hole filling factor R required to obtain effective dielectric constant ϵ_{eff} in the matching layer is given by Kildal et al. (1984) as:

$$R = \frac{(\epsilon+1)(\epsilon-\epsilon_{eff})}{(\epsilon-1)(\epsilon+\epsilon_{eff})}$$

which is derived by solving an electrostatics problem for a uniform array of infinite dielectric cylinders perpendicular to the electric field. To obtain $\epsilon_{eff} = \sqrt{2.08}$, the hole filling factor should be 0.516. We actually used a filling factor of 0.50, which produces an index of refraction of 1.208 vs. the desired value of 1.201.

8. Focus and illumination efficiency calculations

Since the models seem to match the measured beam patterns closely, it is interesting to see if they can also predict the focus shifts and aperture efficiencies we measured when the defective optical components were installed. According to Schroeder (1987, p. 20), displacing the subreflector by ds moves the Cassegrain focus by $-(m^2+1)ds$, where m is the nominal magnification ratio of the subreflector (11.76 in our case). In Schroeder's system $ds < 0$ when the secondary is moved closer to the primary, whereas on our antennas this is reported as a positive offset. Thus, we assume that the effective Cassegrain focal length F (in inches) is given by $F = 1186'' + (139.29/25.4) \times dx$, where dx is the subreflector offset in mm.

The script in Appendix B computes the illumination efficiency as a function of subreflector position for the 3 different optical configurations (bad window + bad lens, good window + bad lens, good window + good lens). The results agree reasonably well with the measurements made at Hat Creek, but suggest that the optimum focus for the case of the good window + bad lens was -0.5 mm, not -1.0 mm as we actually used.

REFERENCES

Kildal, P.S., Jakobsen, K, & Rao, S. 1984, *Meniscus-lens-corrected corrugated horn: a compact feed for a Cassegrain antenna*, IEE Proceedings, 131, part H, 390.

Lugten, J.B. 1995, *Optical Design and Performance of the BIMA Interferometer*, BIMA memo 39.

Hudson, J.A. 1998, *Ray-tracing the BIMA Reflectors*, BIMA memo 64 (Note: the calculations in this memo assume that the Cassegrain focus is 18 inches behind the vertex of the primary mirror; the correct value is 24 inches. This error does not affect the conclusions of the memo, however.)

Padman, R., Murphy, J.A., & Hills, R.E. 1987, *Gaussian mode analysis of Cassegrain antenna efficiency*, IEEE Transactions, AP-35, 1093–1103.

Schroeder, D.J. 1987, *Astronomical Optics*, New York: Academic Press.

Wylde, R.J. 1984, *Millimetre-wave Gaussian beam-mode optics and corrugated feed horns*, IEE Proceedings, 131, part H, 258–262

This preprint was prepared with the AAS LaTeX macros v4.0.

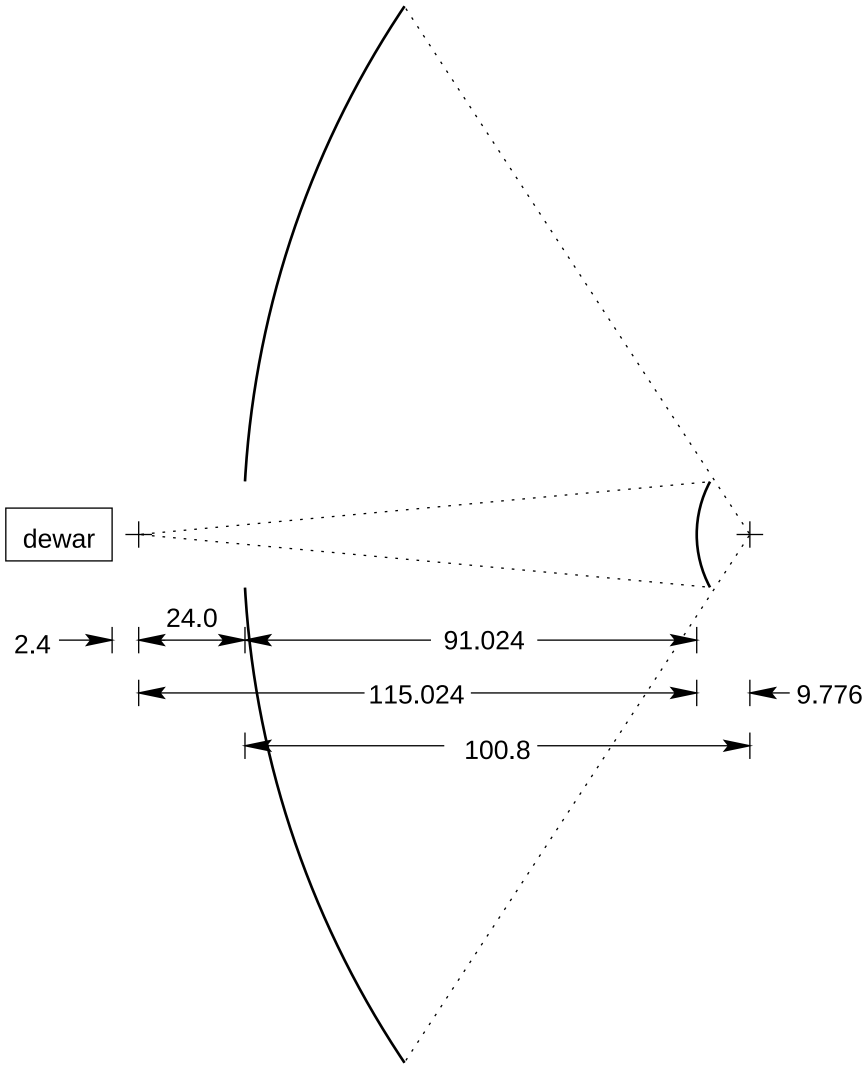

Fig. 1.— BIMA antenna optics. All dimensions are in inches; they are taken from a memo by John Lugten dated 28 May 1991. The front face of the dewar is located 2.4″ behind the Cassegrain focus, which in turn is located 24″ behind the vertex of the primary mirror. The primary mirror is a 240″ diameter paraboloid with focal length 100.8″ ; the equation for its surface is:

$$z = \frac{r^2}{403.2}.$$

The subreflector is a 24″ diameter hyperboloid with first and second focal lengths 9.776446″ and 115.023555″; the equation for its surface is:

$$\left(\frac{z}{52.623554} - 1\right)^2 - \left(\frac{r}{33.533886}\right)^2 = 1$$

The subreflector magnification $m = f_2/f_1$ is 11.7654, the telescope's effective focal length $m \times 100.8$ is 1185.95″, and the plate scale at the Cassegrain focus is 2.90 arcminutes/inch.

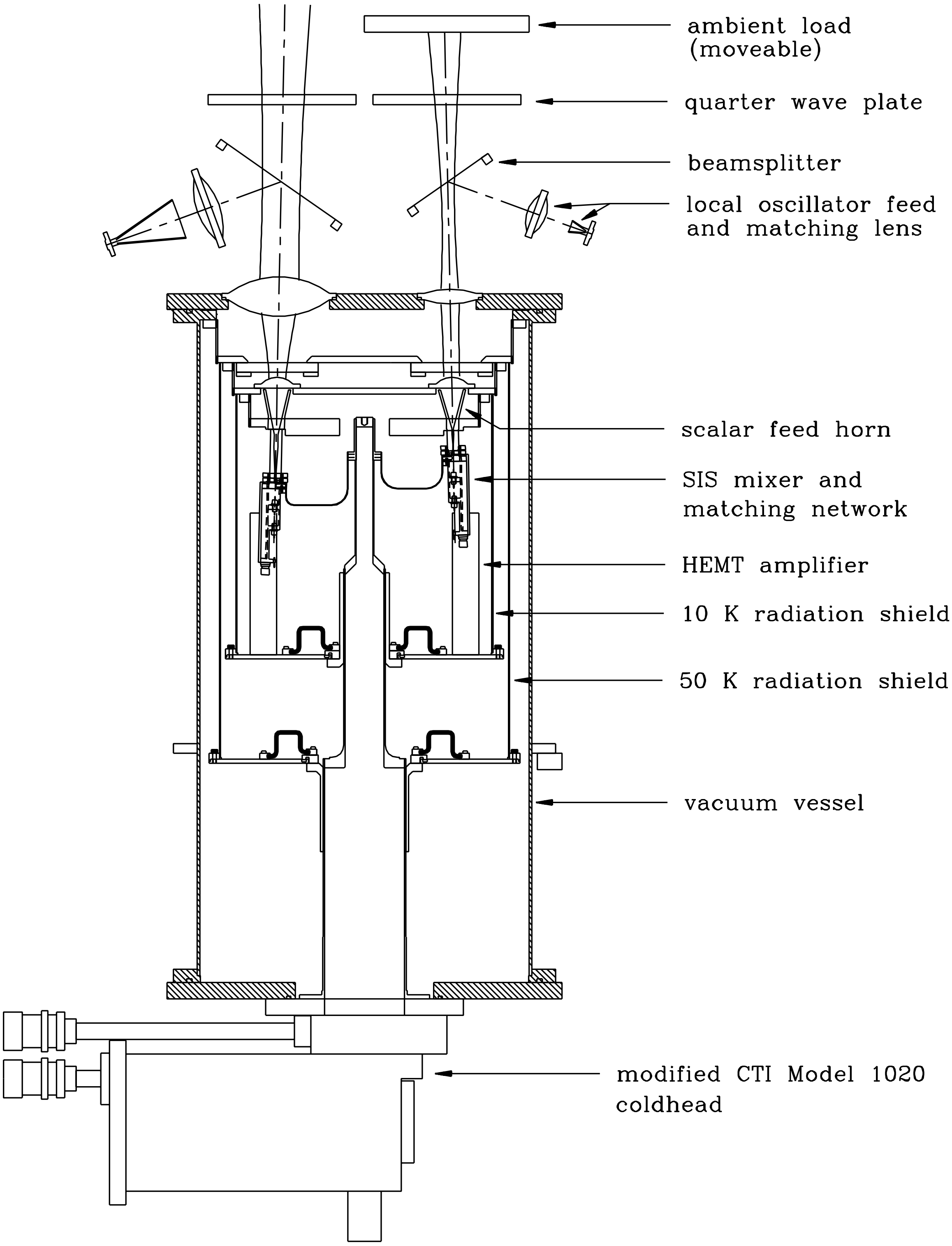

Fig. 2.— Dewar and optics layout for the BIMA receiver. Two of the 4 possible frequency bands are shown. The feed horns for all frequency bands are mounted off-axis.

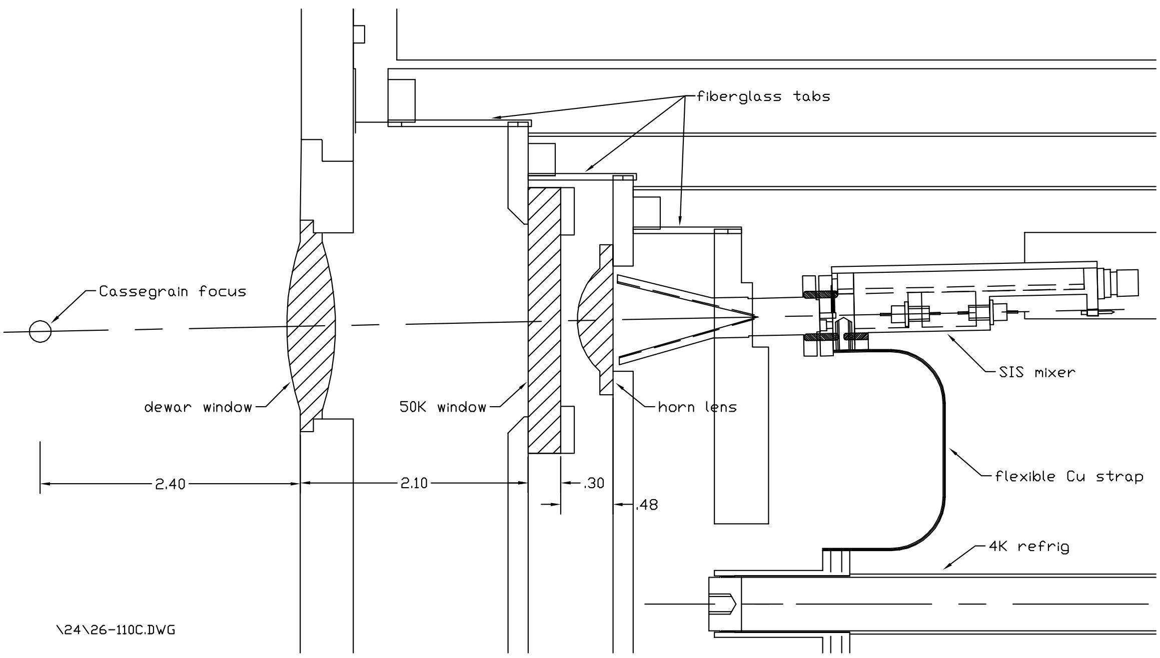

Fig. 3.— Dewar optics for the 1mm band. The telescope's Cassegrain focus is 2.40″ in front of the front surface of the dewar (2.50″ in front of the midplane of the first lens, which also serves as a dewar vacuum window). The center of the feedhorn aperture is 2.655″ off-axis. The horn, which is maintained at 4 Kelvin, is clamped at an angle of 1.17 degrees with respect to the central axis of the dewar. The central ray from the horn passes through the Cassegrain focus 2.546″ off-axis, and intersects the telescope's optical axis 124.5″ from the focus, in the telescope's exit pupil (see Schroeder 1987, pp. 18-19), approximately at the focus of the primary mirror. The horn lens is clamped to the 15 K radiation shield, while a flat piece of Teflon serving as an infrared filter is clamped to the 50 K radiation shield. To maintain optical alignment, the feedhorn clamp ring and both radiation shields are mounted to the front flange of the dewar with sets of fiberglass tabs; connections to the 4 K refrigerator are made with flexible copper straps.

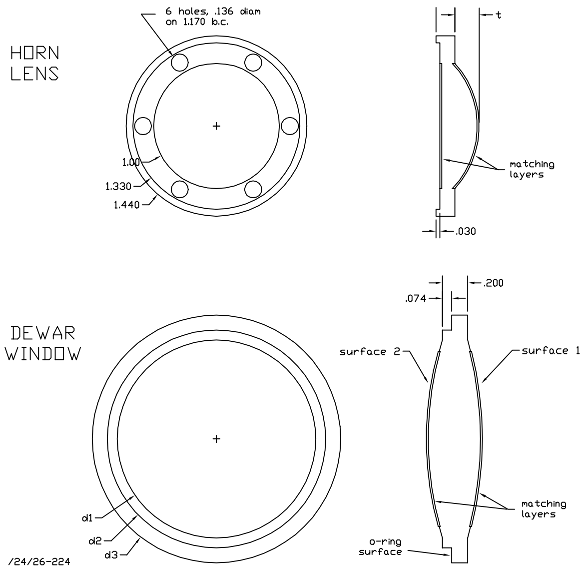

Fig. 4.— Lens dimensions for both the 1mm and 3mm bands. The lens surfaces were designed by ray-tracing with program BEAM3. The horn lenses operate at a temperature of 15 K; according to John Lugten's notes, these lenses were designed assuming a cold index of refraction $n = 1.469$, then the dimensions were scaled upward by a factor of 1.0239 so the lens would shrink to the correct size when cooled. Matching layers on the new horn lenses are grids of holes, as discussed in section 7; matching layers on the dewar windows are concentric grooves. The table below gives the lens dimensions and the approximate focal length $f = R/(1.442 - 1)$ of each surface, where R is a fit, by eye, to the radius of curvature near the center of the lens. The surfaces are defined by the equation

$$z(r) = \frac{cr^2}{1 + \sqrt{1 - sc^2r^2}} + a_4r^4 + a_6r^6 + a_8r^8 + a_{10}r^{10}$$

	1mm			3mm		
	horn lens	dewar lens		horn lens	dewar lens	
		surf 1	surf 2		surf1	surf2
c	1.45537	.36829	.42956	1.21386	.43786	.39337
s	-.32107	-1.98999	-.30488	-.29075	.16395	-3.13973
a4	.26911	0.00000	.00000	.14593	.00000	.00000
a6	.00818	-.00022	.00008	.00483	.00004	-.00103
a8	.03550	.00006	-.00001	.00819	.00000	.00041
a10	.00000	-.00001	.00000	.00000	.00000	-.00007
t	.192	.110	.133	.156	.530	.377
f	1.63	6.33	5.43	1.92	5.43	6.56
d1	1.00	1.58	1.58	1.00	3.08	3.08

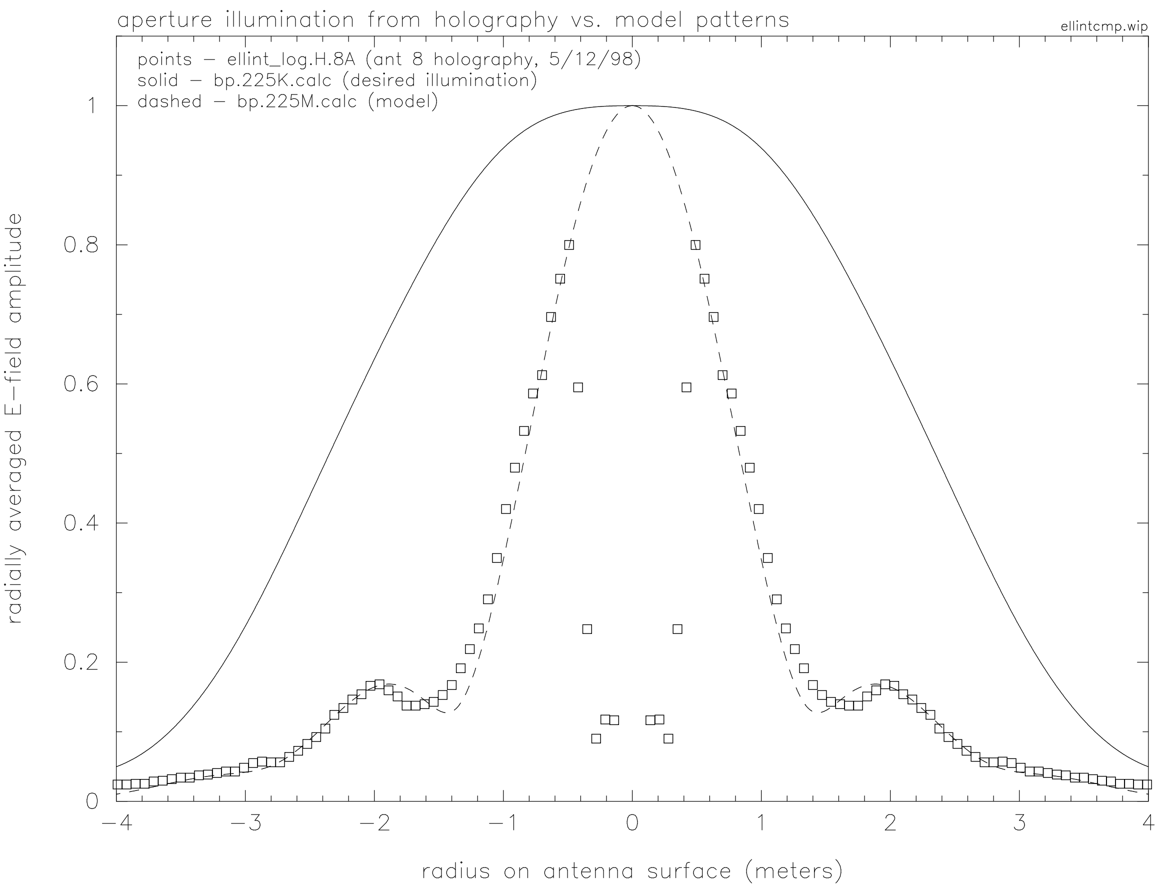

Fig. 5.— Open squares show the E-field amplitude vs radius for antenna 8 at 230 GHz, measured holographically in May 1998 with defective 50 K window and horn lens installed in the receiveer. The voltage pattern across the dish was averaged in annuli with program *ellint* to produce this plot. Blockage by the subreflector causes the hole in the center of the pattern. The solid curve is the theoretically expected E-field, while the dashed curve is a theoretical model incorporating the effects of the defective optical components; the corresponding lab measurement is shown in Figure 9.

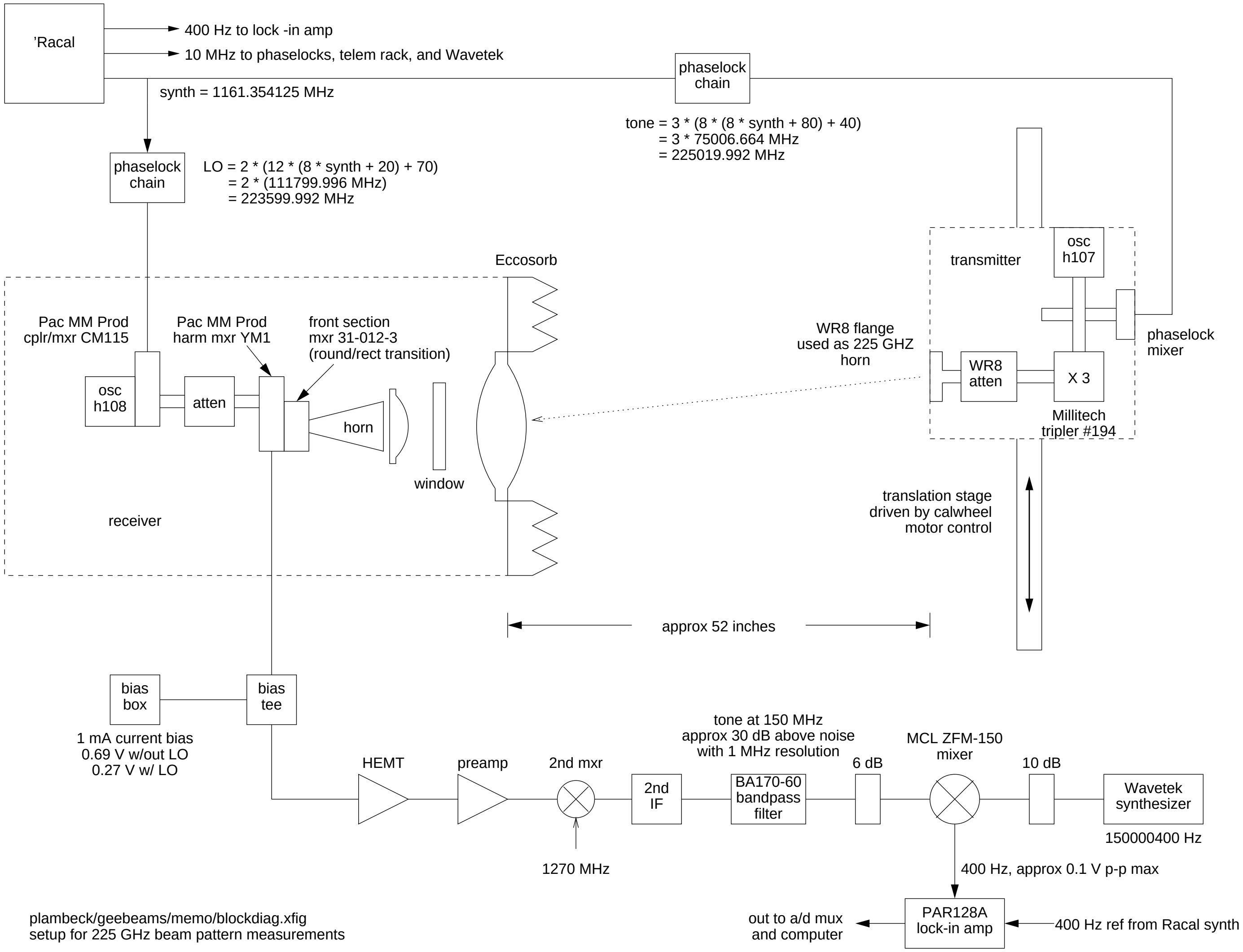

Fig. 6.— Block diagram of the lab test setup.

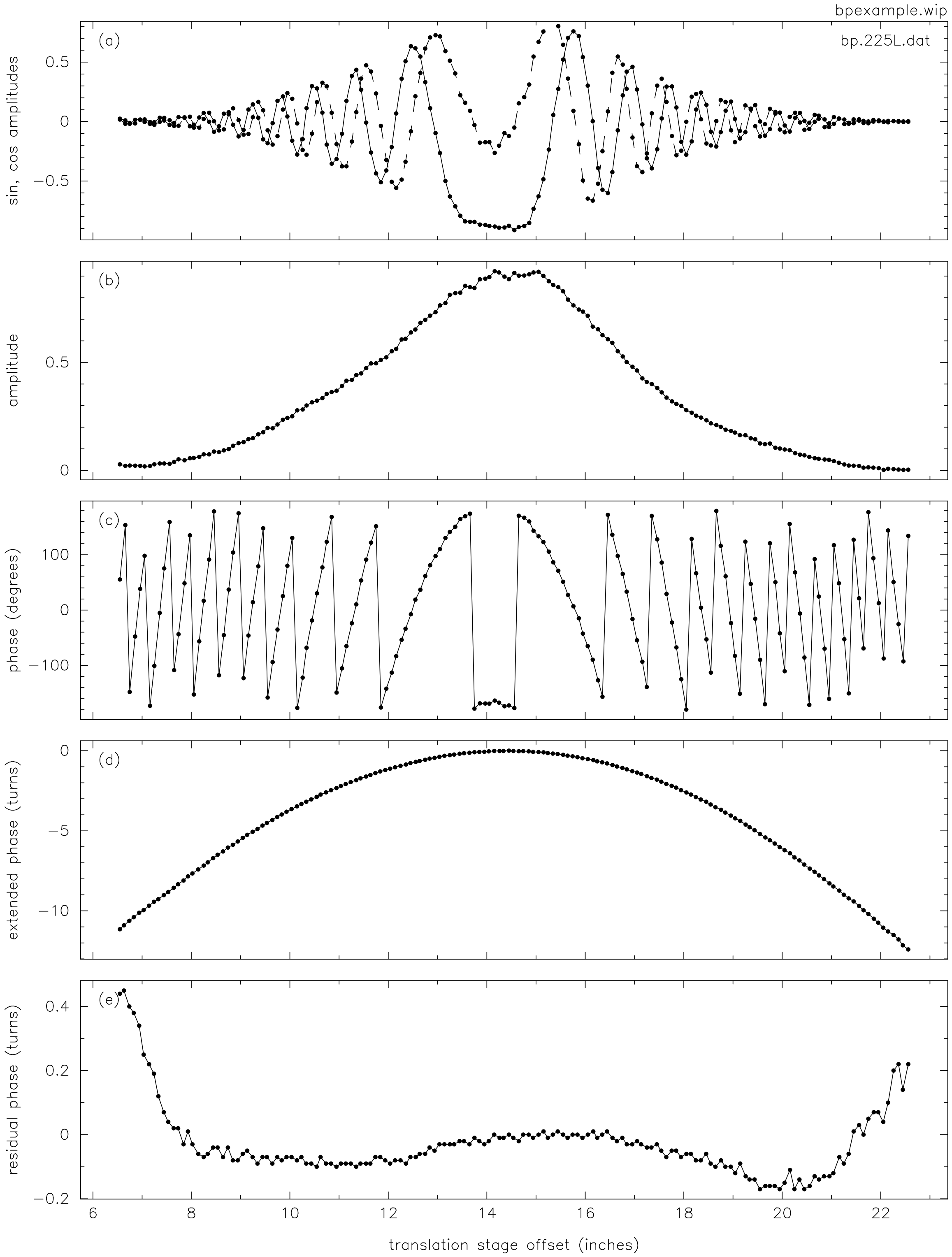

Fig. 7.— Data analysis example. (a) cosine and sine amplitudes; (b) fringe amplitude; (c) fringe phase; (d) phases extended through $\pm\pi$; (e) residual phase after removing a spherical wavefront.

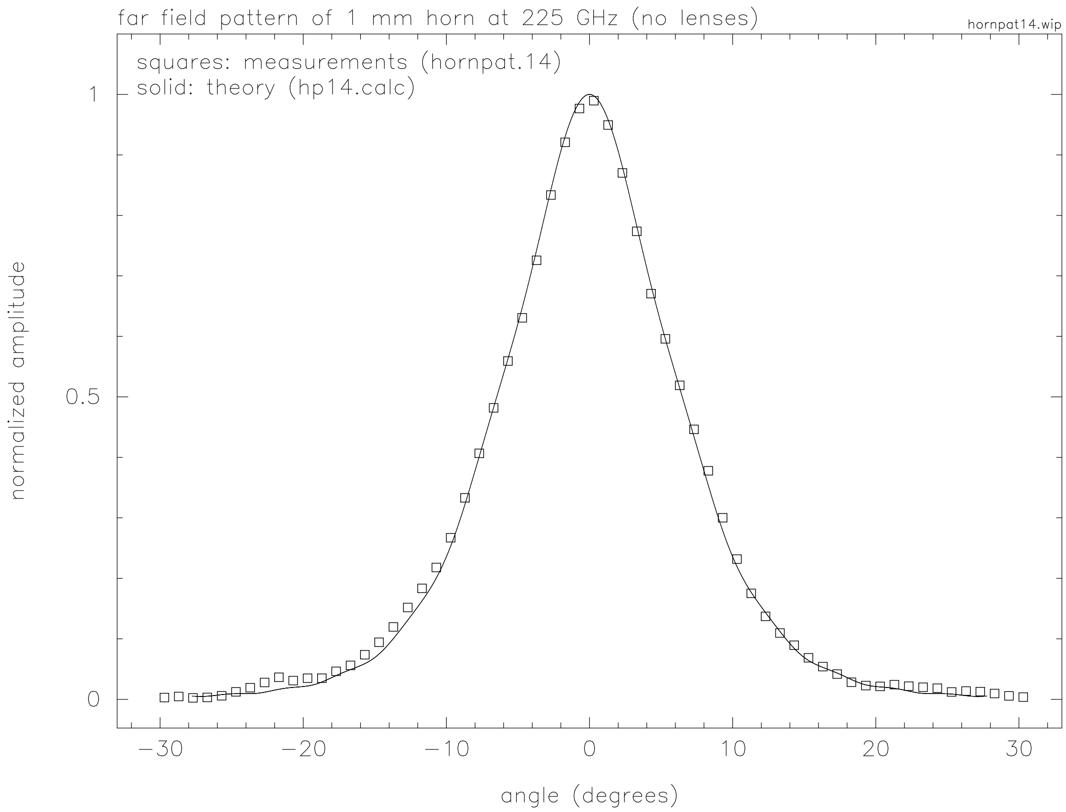

Fig. 8.— Beam pattern of the 1mm feed horn with no lenses. Points show the measured amplitudes, while the solid curve shows the theoretical prediction, generated using the script given in Appendix A. Because the pattern of the naked horn is so broad, the receiver was mounted on a rotary table and the transmitter was held fixed for this measurement.

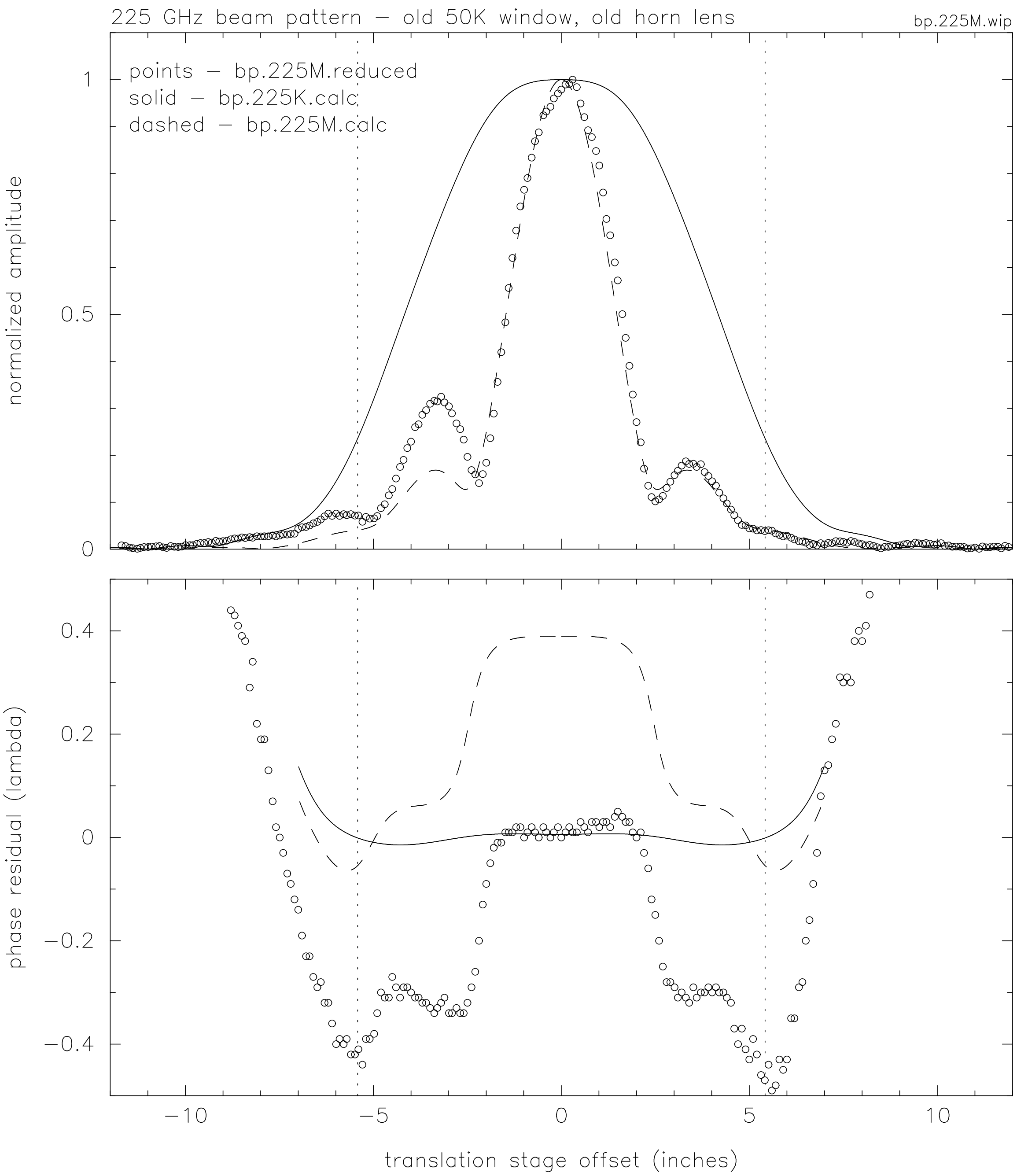

Fig. 9.— Lab measurement of the beam pattern of the full 1mm optical train (dots) using the original horn lens and 50 K window. The solid line shows the expected beam pattern, while the dashed curve shows the pattern predicted if there is a "cusp" in the refractive index of both the horn lens and the 50 K window. The transmitter was 53″ from the receiver for these measurements; vertical dotted lines indicate the section of the pattern which will hit the subreflector, 117.4″ from the receiver. The phase residuals are relative to a circular wavefront expanding from the nominal focus 2.4″ in front of the dewar.

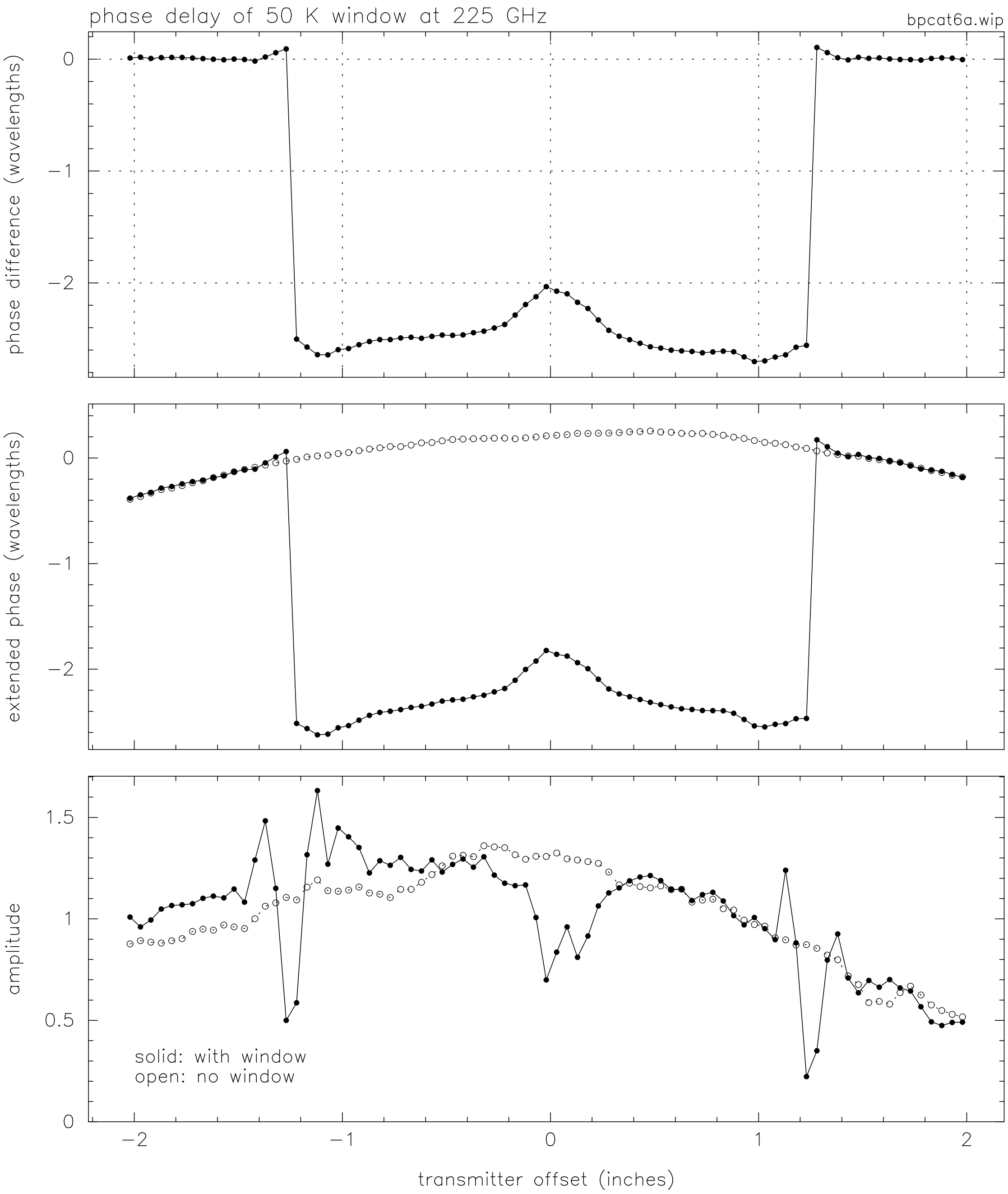

Fig. 10.— Lab measurements of the phase delay through a defective 50 K window. The 2.5″ diameter window was held fixed as close as possible to the transmitter, which was scanned behind it in 0.05″ steps. In this cased the transmitter feed horn was a WR10 waveguide flange, so the resolution is of order 0.10″, the waveguide width. Two scans were done, one with the window present (filled circles), one with it removed (open circles). The top panel shows the phase difference between the two scans. The Teflon window is 0.30″ thick, so it is expected to delay the transmitted signal by $(n-1)t = 2.55\lambda$ at 225 GHz. The measurements show, however, that the delay is only about 2λ along the central axis, indicating that the refractive index is 20% lower at the center of the window.

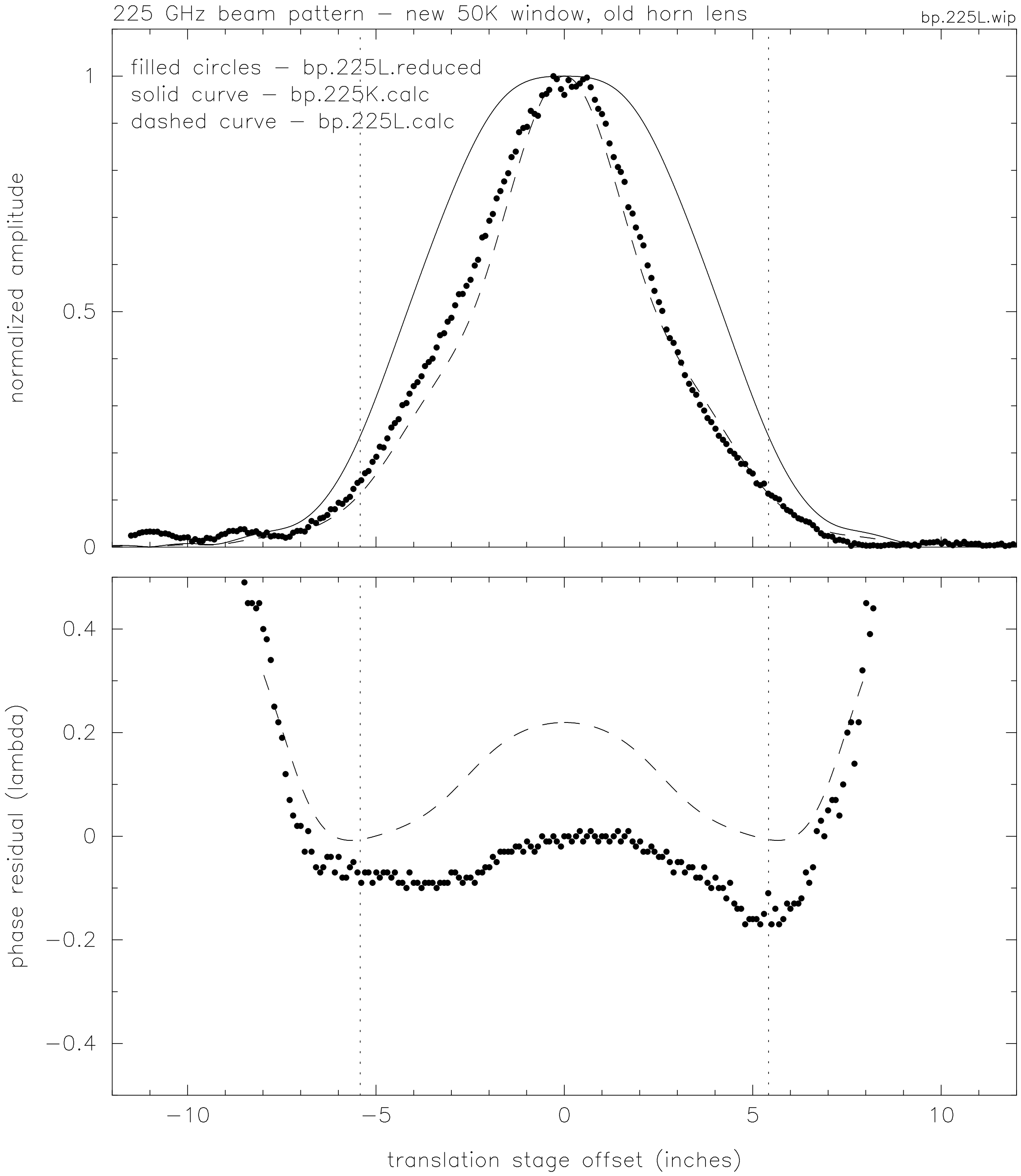

Fig. 11.— Lab measurements of the 1mm receiver beam pattern with a new 50 K window installed. Although greatly improved relative to the pattern in Figure 9, the illumination is still narrower than desired. As in Figure 9, the solid curve shows the desired pattern, while dashed curves show the pattern predicted if there is a "cusp" in the refractive index of the horn lens only. As before, the phase residuals are relative to a circular wavefront expanding from the nominal focus 2.4″ in front of the dewar.

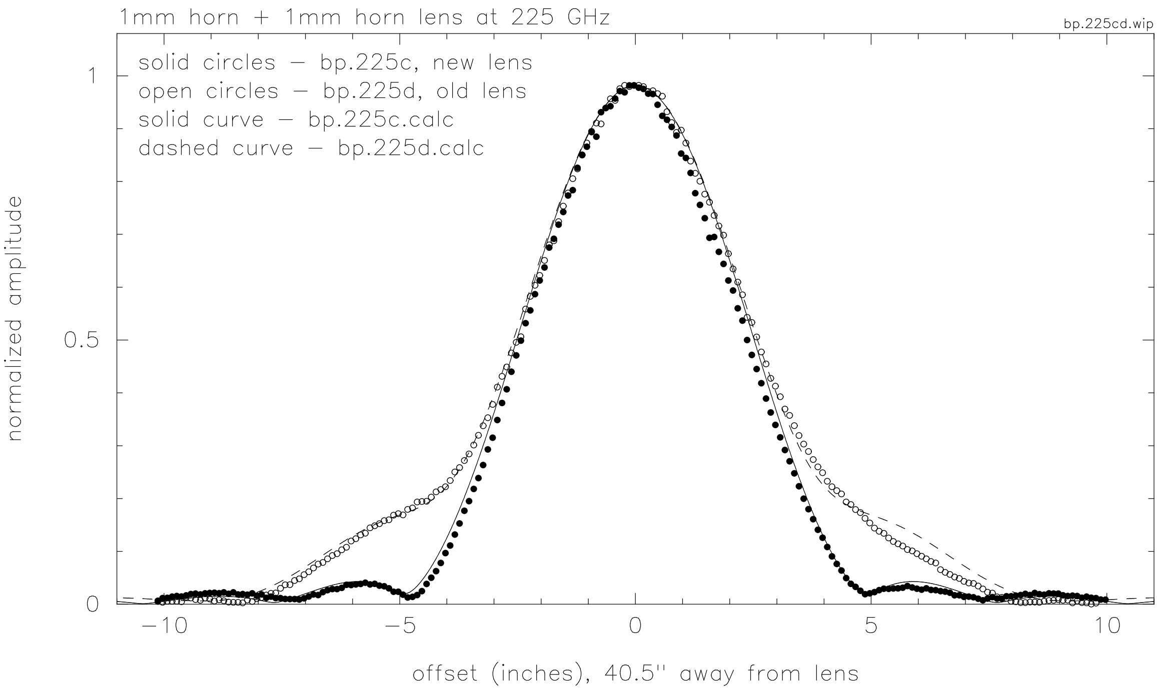

Fig. 12.— Beam pattern of 1mm feed horn + horn lens, for the old and new lenses. The solid curve is the beam pattern expected for an ideal lens. The dashed curve is the theoretical prediction for a defective lens with a cusp in its refractive index.

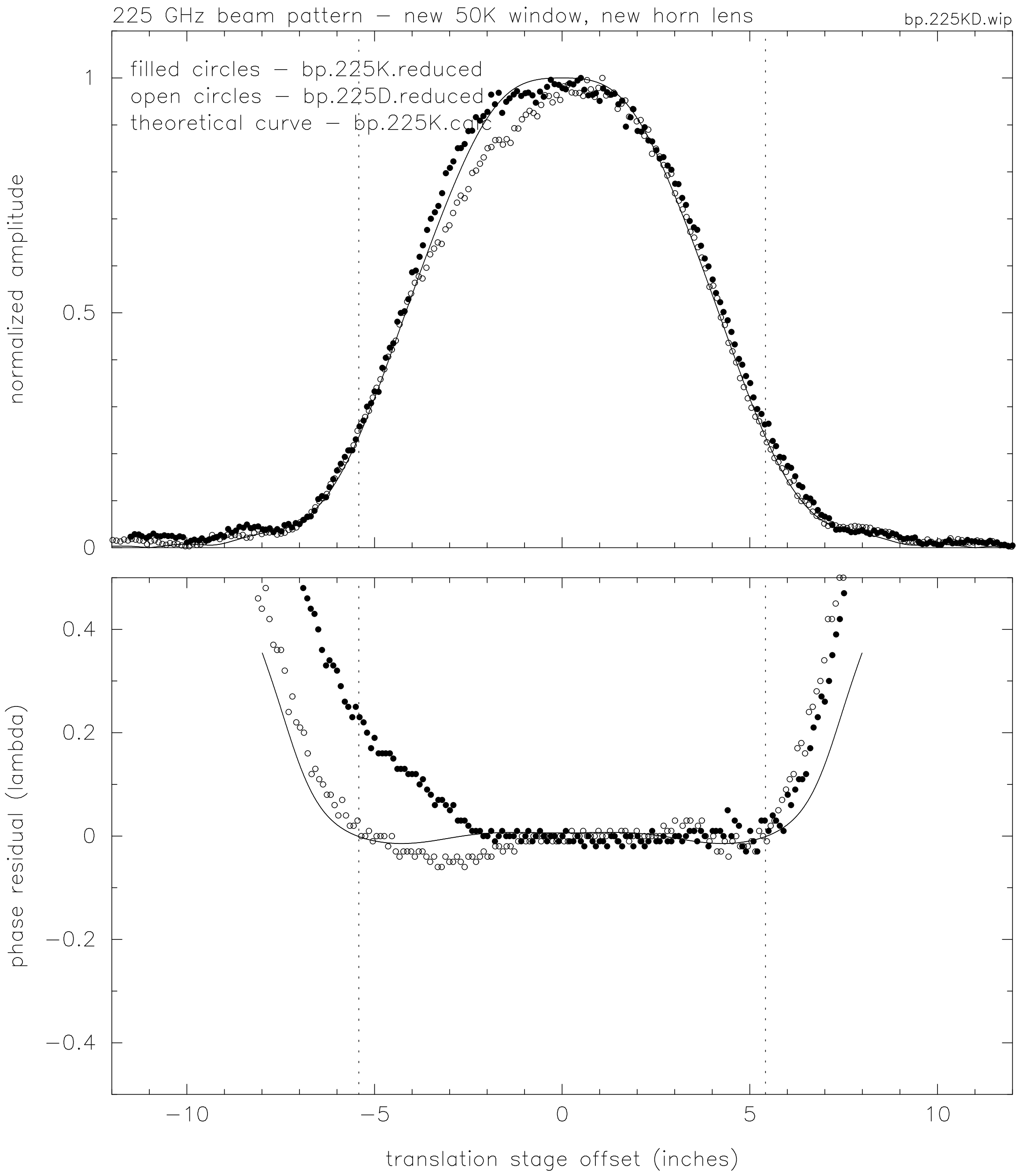

Fig. 13.— Two lab measurements of the beam pattern of the full 1mm optical train using a new 50 K window and a new horn lens. The difference in the two patterns is representative of the variability we found in the lab measurements when the transmitter-receiver separation was changed slightly. It may be caused be standing waves between the transmitter and receiver, or perhaps by mechanical errors in the translation stage. Solid curves show the predicted E-field amplitude and phase.

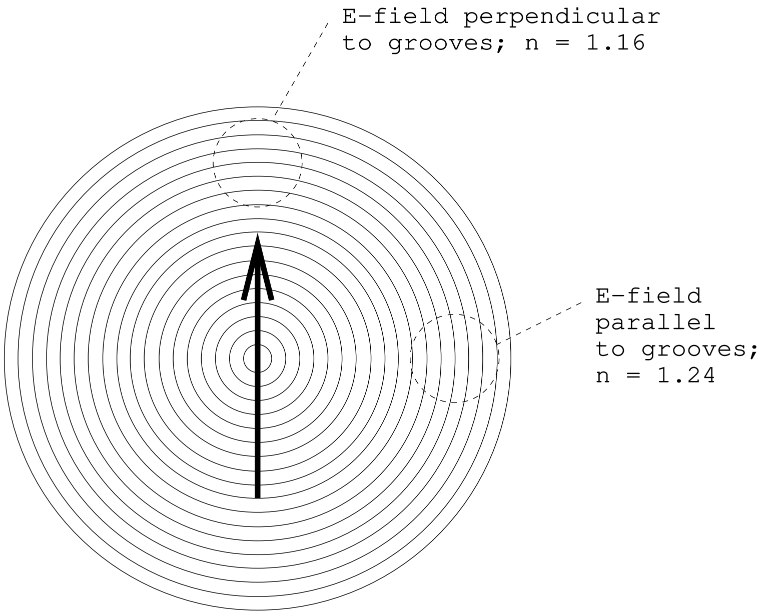

Fig. 14.— Antireflection coating the lenses in the traditional way, with circular grooves, produces a systematic phase error across the lens for linearly polarized signals.

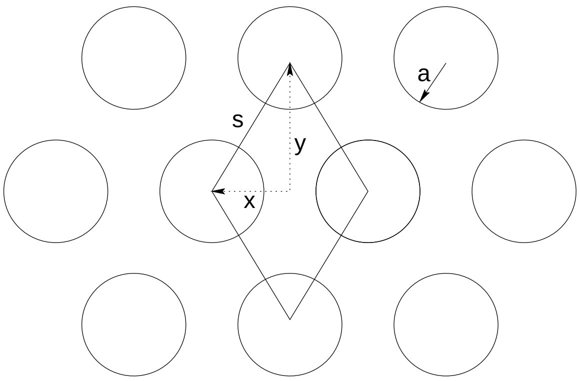

Fig. 15.— Geometry of the antireflection coating. The hole diameter is $2a$ and the hole spacing is s. The unit cell has total area $2xy = (\sqrt{3}/2)s^2$ and contains one hole of area πa^2. Thus, to obtain a hole filling factor of R the holes should be spaced by $s = 0.9523(2a)R^{-0.5}$.

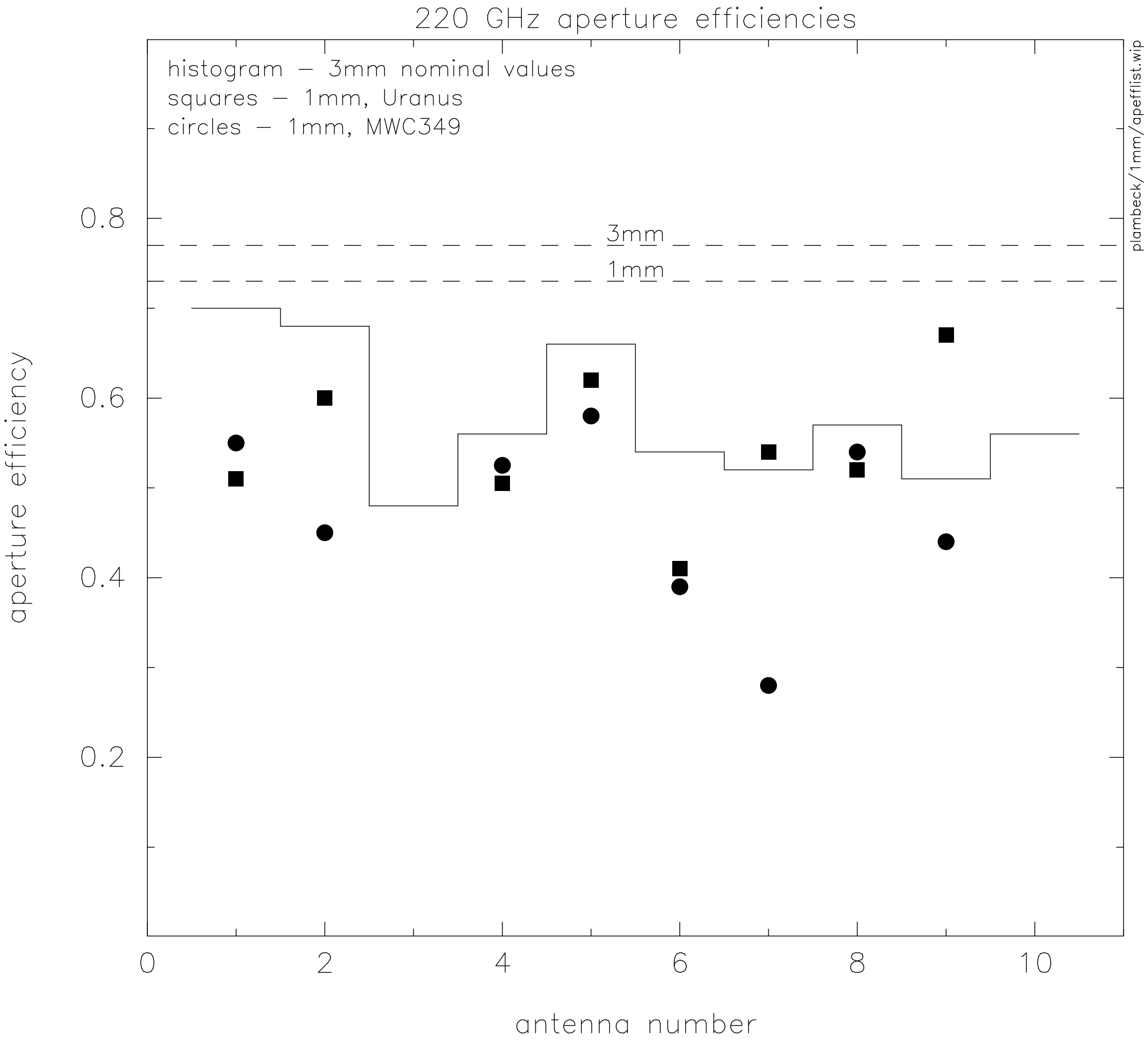

Fig. 16.— Measurements of the telescope aperture efficiencies at 220 GHz, derived from observations of Uranus (squares) and MWC349 (circles) on 9 April 1999 (data set $tt18c220.flux$). The brightness temperature of Uranus was taken to be 94 K, and the continuum flux from MWC349 was assumed to be 1.7 Jy. Dashed lines indicate the theoretically expected values at 3mm and 1mm, while the histogram shows the 3mm values which are actually used by the online software ($\eta = 94.6/jyperka$).

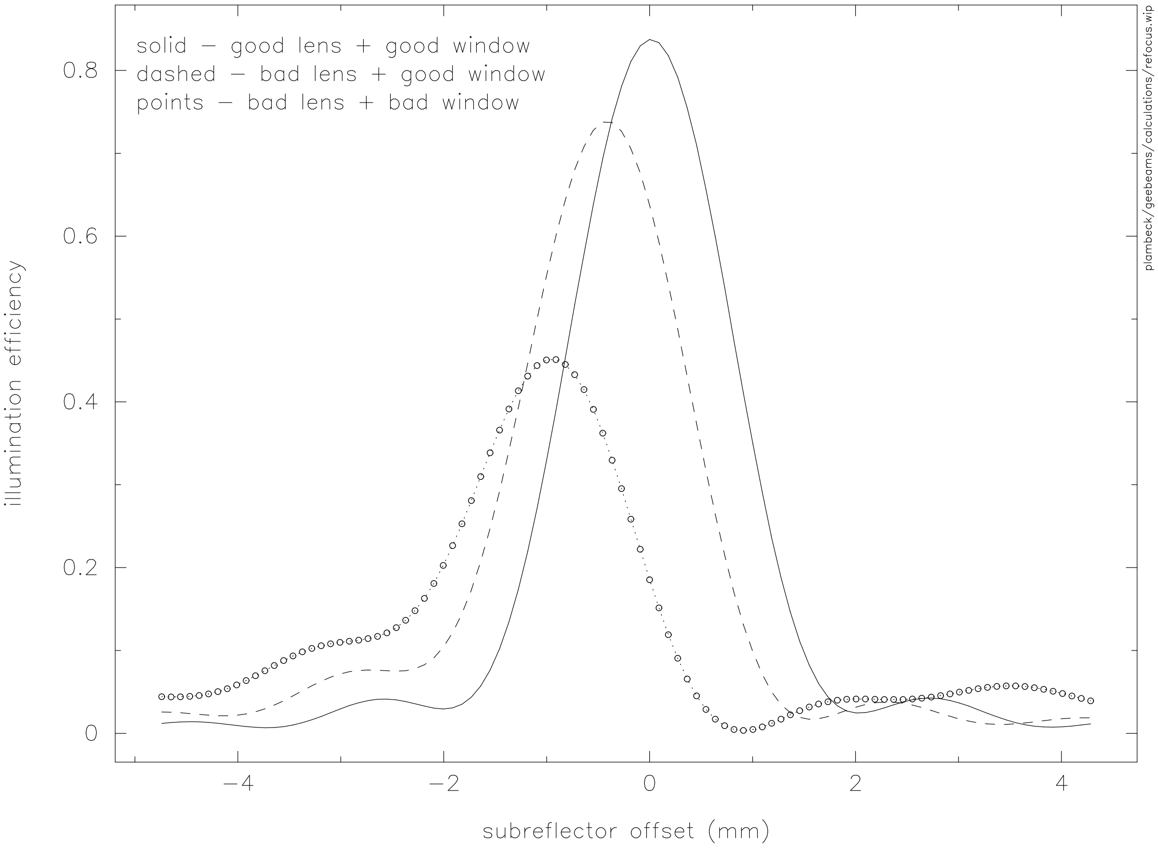

Fig. 17.— Theoretical focus curves generated by the script in Appendix B, for the 3 optics systems. In the table below, peak illumination efficiencies were multiplied by 0.876 (Lugten 1995) to obtain the predicted aperture efficiencies at the best focus. The theoretical aperture efficiencies are somewhat better than those measured.

lens	window	illum eff	ap eff	focus (mm)
good	good	0.84	0.73	0.00
bad	good	0.74	0.65	-0.45
bad	bad	0.45	0.39	-0.95

A. Listing of the Geebeams modelling script

```
#!/bin/csh
# pat.csh
# analyze 1mm optics with geebeams

set lens = good
set window = good

# curved wavefront from scalar feedhorn
# front .052 .222 1.65
  j0 .001 .345 .345 > j0.dat
  modes 100 .222 1.262 .699 < j0.dat > modes.dat

#     compute far field pattern of horn with no lenses
#     front .052 .222 1.65 ... | space 57
      bbeam .01 30 8.963 58.26 .699 < modes.dat > bpat.dat
      nawk -f awkampphs bpat.dat > bp.nakedhorn

# horn lens
# front .052 .222 1.65 ... | space .15 | lens 1.63
  mlens 1.412 .699 -.552 3.463 < modes.dat > modes2.dat
  if ($lens == "bad") then
     bbeam .001 0.7 .242 -.552 3.463 < modes2.dat > bpat.dat
     nawk -f awkcusplens bpat.dat > afterlens.dat
     modes 100 .242 -.552 3.463 < afterlens.dat > modes2.dat
  endif

#     compute pattern of horn + lens measured 40.5" from transmitter
#     front .052 .222 1.65 | space .15 | lens 1.63 ... | space 40.5
      bbeam .01 30 2.772 39.947 3.463 < modes2.dat > bpat.dat
      if ($lens == "bad") then
         nawk -f awkampphs bpat.dat > bp.225d.calc
      else
         nawk -f awkampphs bpat.dat > bp.225c.calc
      endif

# if 50K window is bad, compute pattern .45" beyond horn lens, apply phase cusp,
#   recompute modes
# front .052 .222 1.65 | space .15 | lens 1.63 | space .45
```

```
  if ($window == "bad") then
     bbeam .001 0.8 .240 -.102 3.462 < modes2.dat > bpat.dat
     nawk -f awkcuspwin bpat.dat > afterwindow.dat
     modes 100 .240 -.102 3.463 < afterwindow.dat > modes2.dat
  endif

# dewar window truncates beam at radius of 0.79"; recompute modes
# 50K window shortens effective distance from horn lens to dewar window by 0.09"
  bbeam .001 .79 .271 1.847 3.463 < modes2.dat > bpat.dat
  modes 100 .271 1.847 3.463 < bpat.dat > modes2.dat

# propagate beam through surface 2 of dewar window
# front .052 .222 1.65 | space .15 | lens 1.63 | space 2.5 | lens 5.43
  mlens 1.847 3.463 -1.175 4.112 < modes2.dat > modes3.dat

# propagate beam through surface 1 of dewar window
# front .052 .222 1.65 | space .15 | lens 1.63 | space 2.5 | lens 5.43 | space 0.2
#    | lens 6.33
  mlens -.975 4.112 -2.165 2.345 < modes3.dat > modes4.dat

#     compute beam pattern 53" in front of dewar for comparison with bp.225K,L,M
#     front .052 .222 1.65 | space .15 | lens 1.63 | space 2.5 | lens 5.43 | space 0.2 |
#        lens 6.33 | space 53
      bbeam .01 30 4.275 50.835 2.345 < modes4.dat > bpat.dat
      if (($lens == "good") && ($window == "good")) then
         nawk -f awkampphs bpat.dat > bp.225K.calc
      else if (($lens == "bad") && ($window == "good")) then
         nawk -f awkampphs bpat.dat > bp.225L.calc
      else if (($lens == "bad") && ($window == "bad")) then
         nawk -f awkampphs bpat.dat > bp.225M.calc
      endif

# allow beam to propagate through the entire telescope (effective focal length 1186),
# front .052 .222 1.65 | space .15 | lens 1.63 | space 2.5 | lens 5.43 | space 0.2 |
#   lens 6.33 | space 1188.5 | lens 1186
  mlens 1186.3 2.380 -69032 582963 < modes4.dat > modes5.dat
  bbeam .5 120 98.92 -69032 582963 < modes5.dat > bpat.dat
  nawk -f awkampphs bpat.dat > bp.primary

# find overlap with tophat function to compute theoretical aperture efficiency
  tophole .5 120 .1 > tophole.dat
```

```
  modes 100 98.92 -69032 582963 < tophole.dat > modesin.dat
  echo "aperture efficiency including phase:"
  overlapm modes5.dat modesin.dat

# zero the phase across the aperture and check the aperture efficiency again
  nawk '{print $1, sqrt($2*$2+$3*$3), 0.0}' bpat.dat > bp.nophase
  modes 100 98.92 -69032 582963 < bp.nophase > modes5.dat
  echo "aperture efficiency with phase=0"
  overlapm modes5.dat modesin.dat


# -------------- awkcusplens ------------------- #
BEGIN {rmax = 0.27; phimax = 1.8}
{ if ($1 < rmax) {phi = phimax * (rmax-$1)/rmax; \
           real = $2 * cos(phi) - $3 * sin(phi); \
           imag = $3 * cos(phi) + $2 * sin(phi); \
           print $1, real, imag} \
  else print $0}

# -------------- awkcuspwin -------------------- #
BEGIN {rmax = 0.27; phimax = 2.5}
{ if ($1 < rmax) {phi = phimax * (rmax-$1)/rmax; \
           real = $2 * cos(phi) - $3 * sin(phi); \
           imag = $3 * cos(phi) + $2 * sin(phi); \
           print $1, real, imag} \
  else print $0}

# -------------- awkampphs --------------------- #
{if (NR == 1) a0 = sqrt($2*$2+$3*$3)}
{print $1, sqrt($2*$2+$3*$3)/a0, atan2($3,$2)/6.28318531}
```

B. Listing of refocus.csh

```
#!/bin/csh

# generate pattern of plane wave with subreflector blockage

  tophole .5 120 .1 > tophole.dat

# fix distance from receiver to lens representing the telescope,
# to 1188.5 inches; changing subreflector position by ds changes
# the effective focal length of this lens:
#
#    f = 1186 + (m^2 + 1)ds = 1186 + 139.3 * ds
#
# where m is the telescope magnification (11.76) and ds is the
# offset of the subreflector from its nominal position; in our
# coordinate system ds is positive if the subreflector moves
# TOWARD the primary mirror; allow f to vary from 1170-1200'';
# use Geebeams to find the radius of curvature of the beam in
# the aperture plane of the primary mirror; apply phase correction
#
#    phi = -(r^2/2R)/lambda = - (rmax^2/(2 lambda)/R * (r/rmax)^2
#        = -138461/R * (r/rmax)^2
#
# to the beam pattern(s) computed in appendix A, where phi is in
# turns of phase; find overlap with tophole.dat to find illumination
# efficiency

@ fl = 11600
while ($fl < 12100)
    echo "fl = $fl" > focustmp
    nawk '{printf"front .052 .222 1.65 | space .15 | lens 1.63 | space 2.5 | lens 5.43 \
      | space 0.2 | lens 6.33 | space 1188.5 | lens %8.2f | grep 1/R\n",$3/10.}' \
      focustmp > tmp
    chmod +x tmp
    tmp > tmp2

    nawk '{printf("phasefun .5 120 %f 0. 0. 0. 0. > pf.dat\n",-138461.*$2)}' tmp2 > tmp
    chmod +x tmp
    tmp
```

```
# pf1.dat is pattern with good lens/good window, pf2.dat with good window/bad lens,
# pf3.dat with bad window/bad lens

    mult pf.dat pf1.dat > rf1.dat
    mult pf.dat pf2.dat > rf2.dat
    mult pf.dat pf3.dat > rf3.dat

overlap rf1.dat tophole.dat >> focustmp
overlap rf2.dat tophole.dat >> focustmp
overlap rf3.dat tophole.dat >> focustmp

    more focustmp
nawk '{if (NR == 1) fl = $3; \
       if (NR == 2) eta1 = $2; \
   if (NR == 3) eta2 = $2; \
       if (NR == 4) printf("%7.3f  %7.1f  %6.4f  %6.4f  %6.4f\n", \
(fl-11860.)*.01823,fl/10.,eta1,eta2,$2)}' focustmp >> focus.dat
   @ fl +=  5
end
```